

# Quantum spin-1 anisotropic ferromagnetic Heisenberg model in a crystal field: A variational approach

D. C. Carvalho,<sup>1</sup> J. A. Plascak,<sup>1,2</sup> and L. M. Castro<sup>3</sup><sup>1</sup>*Departamento de Física, Instituto de Ciências Exatas, Universidade Federal de Minas Gerais, Caixa Postale 702, 30123-970 Belo Horizonte, Minas Gerais, Brazil*<sup>2</sup>*Center for Simulational Physics, University of Georgia, 30602 Athens, Georgia, USA*<sup>3</sup>*Departamento de Ciências Exatas, Universidade Estadual do Sudoeste da Bahia, Estrada do Bem Querer Km04, Caixa Postale 95, 45083-900 Vitória da Conquista, Bahia, Brazil*

(Received 27 June 2013; published 6 September 2013)

A variational approach based on Bogoliubov inequality for the free energy is employed in order to treat the quantum spin-1 anisotropic ferromagnetic Heisenberg model in the presence of a crystal field. Within the Bogoliubov scheme an improved pair approximation has been used. The temperature-dependent thermodynamic functions have been obtained and provide much better results than the previous simple mean-field scheme. In one dimension, which is still nonintegrable for quantum spin-1, we get the exact results in the classical limit, or near-exact results in the quantum case, for the free energy, magnetization, and quadrupole moment, as well for the transition temperature. In two and three dimensions the corresponding global phase diagrams have been obtained as a function of the parameters of the Hamiltonian. First-order transition lines, second-order transition lines, tricritical and tetracritical points, and critical endpoints have been located through the analysis of the minimum of the Helmholtz free energy and a Landau-like expansion in the approximated free energy. Only first-order quantum transitions have been found at zero temperature. Limiting cases, such as isotropic Heisenberg, Blume-Capel, and Ising models, have been analyzed and compared to previous results obtained from other analytical approaches as well as from Monte Carlo simulations.

DOI: [10.1103/PhysRevE.88.032111](https://doi.org/10.1103/PhysRevE.88.032111)

PACS number(s): 05.70.Fh, 75.10.Hk, 75.10.Jm

## I. INTRODUCTION

Quantum phase transitions have been extensively studied in the literature [1–7] and their full understanding is still one of the most interesting and important subjects in modern condensed matter physics, both experimentally and theoretically. These transitions have been observed in several experimental realizations such as the magnetic insulators LiHoF<sub>4</sub> [8] and La<sub>2</sub>CuO<sub>4</sub> [9] and the heavy-fermion systems [10] CeRu<sub>2</sub>Si<sub>2</sub> and β-YbAlB<sub>4</sub>. These quantum phase transitions are driven by quantum fluctuations coming from the Heisenberg uncertainty principle (usually due to the existing competition of a field with the ordering energy interaction), unlike the classical phase transitions, which are just driven by thermal fluctuations (temperature). Despite the fact that quantum phase transitions occur only at zero temperature and thus in a region of difficult experimental access, quantum effects can also be seen in a finite temperature region [11]. Hence, it is very important to study, besides the quantum phase transitions themselves at absolute zero temperature, the corresponding phase transitions in the region of low temperatures, in which the quantum effects are certainly still present.

From the theoretical point of view, the simplest nontrivial magnetic model that exhibits quantum phase transitions is the Ising model with a transverse field or, simply, the quantum transverse Ising model. It is the transverse field that competes with the ordering exchange interaction energy. In this case, only the spin-1/2 one-dimensional (1D) version [12,13] can be exactly solved. In addition, this 1D quantum model can be mapped onto a two-dimensional classical Ising model. In general, one has indeed that any  $d$ -dimensional quantum system can be mapped onto an analogous  $(d + 1)$ -dimensional classical model [14].

Another important system, and much richer than the quantum transverse Ising model, is the isotropic Heisenberg model. It has been studied for many years, both in its classical [15,16] and quantum versions [17,18]. Nevertheless, this model can be exactly solved in its classical 1D version [19] and in its quantum spin-1/2 1D version [20]. On the other hand, this model, for spin-1 in one dimension, is not integrable due to the difficulty involved with tackling the noncommutativity of spin operators. Moreover, due a theorem by Mermin and Wagner [21], it has been shown that it is not possible for this system, in one and two dimensions, to present any long-range order at finite temperature.

It is known, however, that in realistic systems one expects to find some degree of anisotropy which can modify the global symmetry of the material, creating thus axes, or even planes, of easy magnetization [22–25]. For instance, the ferromagnetic superconductor UGe<sub>2</sub> [26] exhibits an easy axis anisotropy. Therefore, in any theoretical model, one must consider such features in the Hamiltonian that should describe the phenomenon under study. A suitable model that takes into account such asymmetries is the so-called anisotropic Heisenberg model in the presence of a crystal field (or single ion anisotropy), which can be written as

$$\mathcal{H} = -J \sum_{\langle i,j \rangle} [\eta(S_i^x S_j^x + S_i^y S_j^y) + S_i^z S_j^z] - D \sum_{i=1}^N S_i^{z^2} - H \sum_{i=1}^N S_i^z, \quad (1)$$

where  $J > 0$  is the ferromagnetic exchange interaction between spins  $i$  and  $j$ , the first sum is over pairs of nearest-neighbor sites  $\langle i, j \rangle$ , and  $N$  is the total number of sites of

the lattice. The parameter  $\eta$  measures the degree of the spin interaction anisotropy (this model is also called the  $XXZ$  model) in the region of the easy axis for  $\eta < 1$ , or the easy plane for  $\eta > 1$ , and  $D$  plays the role of the crystal field.  $H$  is the external magnetic field which will be set to zero and  $S_i^\alpha$  are the  $\alpha = x, y, z$  components of spin operators at site  $i$  with the eigenvalues of  $S_i^z$  operator taking the values  $-S, -S + 1, \dots, S - 1, S$ .

The above model has some interesting limits: (i) for  $\eta = 0$  it reduces to the classical Blume-Capel model with general spin- $S$ ; (ii) for  $\eta = 1$ ,  $D = 0$ , and  $H = 0$ , one has the isotropic Heisenberg model; and (iii) when  $D \rightarrow \infty$  the Hamiltonian is equivalent to the spin-1/2 Ising model. The classical model in item (i) has been extensively studied, for instance, by mean-field approximations [27–30], mean-field renormalization group [31], Monte Carlo simulations [32–34], and conformal invariance [35], among others. The phase diagram consists of ordered and disordered phases separated by second- and first-order transition lines, with tricritical and double critical end points for integer values of  $S$  (except for  $S = 1$  which has only one tricritical point), and only double critical end points for semi-integer values of the spin  $S$ .

We will consider herein spin  $S = 1$  in order to study the crystal field effects on the quantum model when  $\eta \neq 0$ . In particular, it will also be interesting to better understand how the quantum fluctuations will affect the presence of the tricritical points, mainly for the three-dimensional (3D) lattice. It should be stressed that experimental realizations of spin-1 systems range from metamagnet [36] and magnetic materials (see, for instance, Ref. [37] and references therein) to He<sup>3</sup>-He<sup>4</sup> mixtures [38]. On the other hand, from the theoretical point of view, in the  $\eta = 1$  case, limit (ii) above, the spin-1 ferromagnetic isotropic Heisenberg model in the presence of an arbitrary crystal-field potential has been treated by the mean-field approximation [39,40] and a linked-cluster expansion method [41]. However, to the best of our knowledge, the complete Hamiltonian (1) with spin-1 has been treated only by a mean-field-like approach, which does not distinguish either the topology or the dimension of the lattice [40,42]. Moreover, the topologies of the corresponding phase diagrams have not been detailed enough to give a clear picture of all the transitions involved, mainly the quantum phase transitions at zero temperature. It would be worthwhile thus to investigate the behavior of this anisotropic Heisenberg model with a crystal field by taking a better, or more reliable, approach, even in its 1D version. The procedure we will follow is closely related to the variational approach based on Bogoliubov inequality for the free energy [43], within the pair approximation [44], which reproduces exact results in some limiting cases.

The plan of the paper is as follows. In the next section, we present the theoretical approach for getting the free energy and the thermodynamic quantities of interest. In Sec. III we present the numerical results. Some concluding remarks are given in the last section, and in the Appendix some of the analytical equations are presented.

## II. VARIATIONAL APPROACH FOR THE FREE ENERGY

The pair variational procedure and the corresponding thermodynamic functions of interest will be presented below.

The potentiality of the approximation will be discussed by comparing the results in some limiting cases, where exact or more reliable approaches have been previously employed.

### A. Bogoliubov variational approach

The variational approach that will be employed is based on the Bogoliubov inequality for the free energy [43]

$$F \leq F_0 + \langle \mathcal{H} - \mathcal{H}_0(\gamma) \rangle_0 \equiv \Phi(\gamma), \quad (2)$$

where  $\mathcal{H}$  is the Hamiltonian under study (1),  $\mathcal{H}_0(\gamma)$  is a trial Hamiltonian which can be exactly solved and depends on variational parameters designated by  $\gamma$ .  $F$  is the free energy of the system described by  $\mathcal{H}$ ,  $F_0$  is the corresponding free energy of the trial Hamiltonian  $\mathcal{H}_0$ , and the thermal average  $\langle \dots \rangle_0$  is taken over the ensemble defined by  $\mathcal{H}_0$ . The approximate free energy is then given by the minimum of  $\Phi(\gamma)$  with respect to  $\gamma$ , i.e.,  $F \equiv \Phi_{\min}(\gamma)$ .

We will follow herein the pair approximation by Ferreira *et al.* [44] consisting of taking  $n_1$  single free spins and  $n_2$  disconnected pairs of spins distributed on the lattice, in such a way that  $n_1 + 2n_2 = N$ . In this way, the trial Hamiltonian can be written as

$$\mathcal{H}_0 = \mathcal{H}_0^f + \mathcal{H}_0^p, \quad (3)$$

where  $\mathcal{H}_0^f$  and  $\mathcal{H}_0^p$  are the single free spin and pairs of spins contributions, respectively.

As the Hamiltonian (1) has, in principle, either easy-axis (for  $\eta < 1$ ) or easy-plane (for  $\eta > 1$ ) ordering, each term of the above trial Hamiltonian can be chosen as a sum of two parts:

$$\mathcal{H}_0^f = \mathcal{H}_{0\parallel}^f + \mathcal{H}_{0\perp}^f, \quad (4)$$

$$\mathcal{H}_0^p = \mathcal{H}_{0\parallel}^p + \mathcal{H}_{0\perp}^p, \quad (5)$$

where  $\mathcal{H}_{0\parallel}^f$  and  $\mathcal{H}_{0\parallel}^p$  take into account, respectively, the free and pairs of spins ordering along the  $z$  axis, and  $\mathcal{H}_{0\perp}^f$  and  $\mathcal{H}_{0\perp}^p$  take into account the corresponding ordering along the  $xy$  plane. The free and pairs of spins Hamiltonian components can be then written as

$$\mathcal{H}_{0\parallel}^f = - \sum_{\text{free}} [h_1^\parallel S_i^z + D S_i^{z2} + \gamma_1^\parallel S_i^{z2}], \quad (6)$$

$$\begin{aligned} \mathcal{H}_{0\parallel}^p = & - \sum_{\text{pair}} \{ J[\eta \vec{S}_i \cdot \vec{S}_j + (1 - \eta) S_i^z S_j^z] + D(S_i^{z2} + S_j^{z2}) \\ & + h_2^\parallel (S_i^z + S_j^z) + \gamma_2^\parallel (S_i^{z2} + S_j^{z2}) \}, \end{aligned} \quad (7)$$

$$\mathcal{H}_{0\perp}^f = - \sum_{\text{free}} \left\{ \frac{h_1^\perp}{\sqrt{2}} (S_i^x + S_i^y) + D S_i^{z2} + \gamma_1^\perp S_i^{z2} \right\}, \quad (8)$$

$$\begin{aligned} \mathcal{H}_{0\perp}^p = & - \sum_{\text{pair}} \left\{ J[\eta \vec{S}_i \cdot \vec{S}_j + (1 - \eta) S_i^z S_j^z] + D(S_i^{z2} + S_j^{z2}) \right. \\ & \left. + \frac{h_2^\perp}{\sqrt{2}} (S_i^x + S_j^x + S_i^y + S_j^y) + \gamma_2^\perp (S_i^{z2} + S_j^{z2}) \right\}, \end{aligned} \quad (9)$$

where  $h_1^\parallel$ ,  $h_2^\parallel$ ,  $\gamma_1^\parallel$ , and  $\gamma_2^\parallel$  are variational parameters along the parallel direction of the  $z$  axis and  $h_1^\perp$ ,  $h_2^\perp$ ,  $\gamma_1^\perp$ , and  $\gamma_2^\perp$  are variational parameters in the  $xy$  plane. The sum  $\sum_{\text{free}}$  is taken

over all isolated spins and  $\sum_{\text{pair}}$  is taken over all disconnected pairs of spins. A similar choice for the trial Hamiltonian has been proposed by Lara *et al.* [30] in the study of the classical Blume-Capel model, corresponding to the limiting case  $\eta = 0$  in our Hamiltonian (1). In the present paper, we have generalized such a trial Hamiltonian for different values of the anisotropy  $\eta$ , thereby allowing for the presence of quantum fluctuations in the system, which significantly complicates the analysis. In this pair approximation two nearest-neighbor spin fluctuations are taken into account exactly, while in the previous usual mean-field approach no fluctuations at all were considered [40].

From the trial Hamiltonian  $\mathcal{H}_0$ , we can write the partition function  $\mathcal{Z}_0$  as

$$\begin{aligned} \mathcal{Z}_0 &= \text{Tr}(e^{-\beta\mathcal{H}_0}) = \text{Tr}(e^{-\beta(\mathcal{H}_0^f + \mathcal{H}_0^p)}) \\ &= \text{Tr}(e^{-\beta(\mathcal{H}_{0\parallel}^f + \mathcal{H}_{0\parallel}^p + \mathcal{H}_{0\perp}^f + \mathcal{H}_{0\perp}^p)}) = \mathcal{Z}_{0\parallel}^f \mathcal{Z}_{0\parallel}^p \mathcal{Z}_{0\perp}^f \mathcal{Z}_{0\perp}^p, \end{aligned} \quad (10)$$

in which the free Hamiltonian contributions for the partition function are given by

$$\begin{aligned} \mathcal{Z}_{0\parallel}^f &= \text{Tr}(e^{-\beta\mathcal{H}_{0\parallel}^f}) = (\mathcal{Z}_{1\parallel}^f)^{n_1}, \\ \mathcal{Z}_{0\perp}^f &= \text{Tr}(e^{-\beta\mathcal{H}_{0\perp}^f}) = (\mathcal{Z}_{1\perp}^f)^{n_1}, \end{aligned}$$

where  $\beta = 1/k_B T$ , with  $k_B$  the Boltzmann constant. The one-spin  $3 \times 3$  Hamiltonian matrix can be easily diagonalized yielding

$$\begin{aligned} \mathcal{Z}_{1\parallel}^f &= 1 + 2e^{\beta(D+\gamma_1^{\parallel})} \cosh(\beta h_1^{\parallel}), \quad (11) \\ \mathcal{Z}_{1\perp}^f &= e^{\beta(D+\gamma_1^{\perp})} + 2e^{\frac{\beta(D+\gamma_1^{\perp})}{2}} \\ &\quad \times \cosh\left(\frac{\beta\sqrt{(D+\gamma_1^{\perp})^2 + 4(h_1^{\perp})^2}}{2}\right). \end{aligned} \quad (12)$$

Analogously, for the parallel component of the pair Hamiltonian we get

$$\mathcal{Z}_{0\parallel}^p = \text{Tr}(e^{-\beta\mathcal{H}_{0\parallel}^p}) = (\mathcal{Z}_{2\parallel}^p)^{n_2}, \quad (13)$$

$$\begin{aligned} \mathcal{Z}_{2\parallel}^p &= 4e^{\beta(D+\gamma_2^{\parallel})} \cosh(\beta h_2^{\parallel}) \cosh(\beta J \eta) + e^{-\beta[J-2(D+\gamma_2^{\parallel})]} \\ &\quad + 2e^{\beta[J+2(D+\gamma_2^{\parallel})]} \cosh(2\beta h_2^{\parallel}) + 2e^{-\frac{\beta\alpha}{2}} \cosh\left(\frac{\beta\Delta}{2}\right), \\ \alpha &= J - 2(D + \gamma_2^{\parallel}) \quad \text{and} \quad \Delta = \sqrt{\alpha^2 + 8(J\eta)^2}. \end{aligned} \quad (14)$$

The above expression comes from the parallel pair Hamiltonian which is a  $9 \times 9$  matrix that can be analytically diagonalized. A different situation, however, holds for the perpendicular ( $xy$  plane) component of the pair Hamiltonian. In this case we cannot obtain an analytical expression for the nine eigenvalues of the corresponding Hamiltonian and we have to resort to a numerical diagonalization of  $\mathcal{H}_{0\perp}^p$  in order to get the partition function  $\mathcal{Z}_{0\perp}^p$ .

After calculating the terms appearing in the Bogoliubov inequality, we can write the free energy per particle as

$$f = \frac{F}{N} = f_{\parallel} + f_{\perp} = \frac{F_{\parallel}}{N} + \frac{F_{\perp}}{N}, \quad (15)$$

where the free energies  $f_{\parallel}$  and  $f_{\perp}$  are given by

$$\begin{aligned} f_{\parallel} &= \frac{F_{\parallel}}{N} = -\frac{c}{2} k_B T \ln \mathcal{Z}_{2\parallel}^p + (c-1) k_B T \ln \mathcal{Z}_{1\parallel}^f \\ &\quad + (1-c)(h_1^{\parallel} m_{\parallel} + \gamma_1^{\parallel} q_{\parallel}) + c(h_2^{\parallel} m_{\parallel} + \gamma_2^{\parallel} q_{\parallel}), \end{aligned} \quad (16)$$

$$\begin{aligned} f_{\perp} &= \frac{F_{\perp}}{N} = -\frac{c}{2} k_B T \ln \mathcal{Z}_{2\perp}^p + (c-1) k_B T \ln \mathcal{Z}_{1\perp}^f \\ &\quad + (1-c)(h_1^{\perp} m_{\perp} + \gamma_1^{\perp} q_{\perp}) + c(h_2^{\perp} m_{\perp} + \gamma_2^{\perp} q_{\perp}), \end{aligned} \quad (17)$$

where  $c$  is the coordination number of the lattice. In the above equations  $m_{\parallel}$  and  $m_{\perp}$  are the parallel and perpendicular components of the magnetization defined by

$$m_{\parallel} \equiv \langle S_i^z \rangle_0 = \frac{1}{\beta} \frac{\partial \ln \mathcal{Z}_{1\parallel}^f}{\partial h_1^{\parallel}} = \frac{1}{2\beta} \frac{\partial \ln \mathcal{Z}_{2\parallel}^p}{\partial h_2^{\parallel}}, \quad (18)$$

$$m_{\perp} \equiv \sqrt{\langle S_i^x \rangle_0^2 + \langle S_i^y \rangle_0^2} = \frac{1}{\beta} \frac{\partial \ln \mathcal{Z}_{1\perp}^f}{\partial h_1^{\perp}} = \frac{1}{2\beta} \frac{\partial \ln \mathcal{Z}_{2\perp}^p}{\partial h_2^{\perp}}. \quad (19)$$

Note from Eqs. (18) and (19) that the magnetization coming from single spins and from pairs of spins are the same in order to keep the translational symmetry of the model. Similarly, we get for the parallel and perpendicular components of the quadrupole moments  $q_{\parallel}$  and  $q_{\perp}$

$$q_{\parallel} \equiv \langle S_i^{z^2} \rangle_0 = \frac{1}{\beta} \frac{\partial \ln \mathcal{Z}_{1\parallel}^f}{\partial \gamma_1^{\parallel}} = \frac{1}{2\beta} \frac{\partial \ln \mathcal{Z}_{2\parallel}^p}{\partial \gamma_2^{\parallel}}, \quad (20)$$

$$q_{\perp} \equiv \langle S_i^{z^2} \rangle_0 = \frac{1}{\beta} \frac{\partial \ln \mathcal{Z}_{1\perp}^f}{\partial \gamma_1^{\perp}} = \frac{1}{2\beta} \frac{\partial \ln \mathcal{Z}_{2\perp}^p}{\partial \gamma_2^{\perp}}. \quad (21)$$

After minimizing the free-energy  $f$  with respect to the eight variational parameters  $h_1^{\parallel}, h_2^{\parallel}, \gamma_1^{\parallel}$ , and  $\gamma_2^{\parallel}$ , and  $h_1^{\perp}, h_2^{\perp}, \gamma_1^{\perp}$ , and  $\gamma_2^{\perp}$ , we obtain the following relations

$$(c-1)h_1^{\parallel} = ch_2^{\parallel} \quad \text{and} \quad (c-1)\gamma_1^{\parallel} = c\gamma_2^{\parallel}, \quad (22)$$

$$(c-1)h_1^{\perp} = ch_2^{\perp} \quad \text{and} \quad (c-1)\gamma_1^{\perp} = c\gamma_2^{\perp}. \quad (23)$$

Thus, for a given value of the Hamiltonian parameters  $D/J$ ,  $\eta$ , and  $c$ , and at a reduced temperature  $t = \frac{k_B T}{J}$ , one can solve Eqs. (18)–(23) in order to get the dimensionless reduced variational parameters  $h_1^{\parallel}/J$ ,  $h_2^{\parallel}/J$ ,  $\gamma_1^{\parallel}/J$ , and  $\gamma_2^{\parallel}/J$ , and  $h_1^{\perp}/J$ ,  $h_2^{\perp}/J$ ,  $\gamma_1^{\perp}/J$ , and  $\gamma_2^{\perp}/J$ . When more than one set of solutions are found, the stable solutions will be those which minimize the approximated free energy. From this procedure all thermodynamic properties of the system can be computed.

It turns out that the system is only ordered either along the  $z$  direction or in the  $xy$  plane, in such a way that the variational parameters along  $z$  and perpendicular to  $z$  are decoupled. This allows one to get some analytical results for the critical lines and the tricritical and tetracritical points. For instance, when the perpendicular variational parameters vanish, Eqs. (18) and

(20) yield

$$\frac{e^{\beta\gamma_1^\parallel} \sinh(\beta h_1^\parallel)}{\mathcal{Z}_{1\parallel}^f} = \frac{e^{\beta\gamma_2^\parallel} \sinh(\beta h_2^\parallel)}{\mathcal{Z}_{2\parallel}^p} [2e^{\beta(J+D+\gamma_2^\parallel)} \cosh(\beta h_2^\parallel) + \cosh(\beta J\eta)], \quad (24)$$

$$\frac{2e^{\beta(D+\gamma_1^\parallel)} \cosh(\beta h_1^\parallel)}{\mathcal{Z}_{1\parallel}^f} = \frac{e^{\beta(D+\gamma_2^\parallel)}}{\mathcal{Z}_{2\parallel}^p} \left\{ 2 \cosh(\beta h_2^\parallel) \cosh(\beta J\eta) + e^{\beta(J+D+\gamma_2^\parallel)} [2 \cosh(2\beta h_2^\parallel) + e^{-2\beta J}] + e^{-\frac{\beta J}{2}} \left[ \cosh\left(\frac{\beta\Delta}{2}\right) - \frac{\alpha}{\Delta} \sinh\left(\frac{\beta\Delta}{2}\right) \right] \right\}, \quad (25)$$

which together with Eqs. (22) can be numerically resolved for  $h_1^\parallel(t)/J$ ,  $h_2^\parallel(t)/J$ ,  $\gamma_1^\parallel(t)/J$ , and  $\gamma_2^\parallel(t)/J$ , as a function of the reduced temperature  $t$  for a given set of Hamiltonian parameters. This gives the ordering of the parallel order-parameter  $m_\parallel$  and the thermodynamics of the parallel ordered phase.

At criticality, Eqs. (24) and (25) can be simplified, because the magnetization along the  $z$  axis continuously goes to zero, i.e.,  $m_\parallel \rightarrow 0$ , which is equivalent to taking the limit  $h_1^\parallel \rightarrow 0$  and  $h_2^\parallel \rightarrow 0$ . Hence, we arrive at the following coupled

equations for the critical temperature of the parallel order parameter

$$\frac{e^{\beta\gamma_1^\parallel} c}{(c-1)\mathcal{Z}_{1\parallel}^f(0)} = \frac{e^{\beta\gamma_2^\parallel}}{\mathcal{Z}_{2\parallel}^p(0)} [2e^{\beta(J+D+\gamma_2^\parallel)} + \cosh(\beta J\eta)]$$

and

$$\frac{2e^{\beta(D+\gamma_1^\parallel)}}{\mathcal{Z}_{1\parallel}^f(0)} = \frac{e^{\beta(D+\gamma_2^\parallel)}}{\mathcal{Z}_{2\parallel}^p(0)} \left\{ 2 \cosh(\beta J\eta) + e^{\beta(J+D+\gamma_2^\parallel)} [2 + e^{-2\beta J}] + e^{-\frac{\beta J}{2}} \left[ \cosh\left(\frac{\beta\Delta}{2}\right) - \frac{\alpha}{\Delta} \sinh\left(\frac{\beta\Delta}{2}\right) \right] \right\},$$

where

$$\mathcal{Z}_{1\parallel}^f(0) = 1 + 2e^{\beta(D+\gamma_1^\parallel)}, \quad (26)$$

$$\mathcal{Z}_{2\parallel}^p(0) = 4e^{\beta(D+\gamma_2^\parallel)} \cosh(\beta J\eta) + e^{-\beta[J-2(D+\gamma_2^\parallel)]} + 2e^{\beta[J+2(D+\gamma_2^\parallel)]} + 2e^{-\frac{\beta\alpha}{2}} \cosh\left(\frac{\beta\Delta}{2}\right). \quad (27)$$

Analogously, for the perpendicular plane the same method can be realized to get the perpendicular variational parameters, since in this case the parallel ones vanish. The expressions for  $\frac{1}{\beta} \frac{\partial \ln \mathcal{Z}_{1\perp}^f}{\partial h_1^\perp}$  and  $\frac{1}{\beta} \frac{\partial \ln \mathcal{Z}_{1\perp}^f}{\partial \gamma_1^\perp}$  can be readily obtained from Eq. (12) as follows

$$\frac{1}{\beta} \frac{\partial \ln \mathcal{Z}_{1\perp}^f}{\partial h_1^\perp} = \frac{4e^{\frac{\beta(D+\gamma_1^\perp)}{2}} \sinh\left(\frac{\beta\sqrt{(D+\gamma_1^\perp)^2+4(h_1^\perp)^2}}{2}\right) \frac{h_1^\perp}{\sqrt{(D+\gamma_1^\perp)^2+4(h_1^\perp)^2}}}{\mathcal{Z}_{1\perp}^f}, \quad (28)$$

$$\frac{1}{\beta} \frac{\partial \ln \mathcal{Z}_{1\perp}^f}{\partial \gamma_1^\perp} = \frac{e^{\beta(D+\gamma_1^\perp)} + e^{\frac{\beta(D+\gamma_1^\perp)}{2}} \left[ \cosh\left(\frac{\beta\sqrt{(D+\gamma_1^\perp)^2+4(h_1^\perp)^2}}{2}\right) + \frac{(D+\gamma_1^\perp) \sinh\left(\frac{\beta\sqrt{(D+\gamma_1^\perp)^2+4(h_1^\perp)^2}}{2}\right)}{\sqrt{(D+\gamma_1^\perp)^2+4(h_1^\perp)^2}} \right]}{\mathcal{Z}_{1\perp}^f}. \quad (29)$$

Nevertheless, as previously stressed, the pair perpendicular Hamiltonian  $\mathcal{H}_{0\perp}^p$  could not be solved analytically, meaning we do not have any analytical expression for  $\frac{1}{2\beta} \frac{\partial \ln \mathcal{Z}_{2\perp}^p}{\partial h_2^\perp}$  and  $\frac{1}{2\beta} \frac{\partial \ln \mathcal{Z}_{2\perp}^p}{\partial \gamma_2^\perp}$ . Everything must be done numerically for finite values of  $h_1^\perp$  as  $h_2^\perp$ . However, at criticality,  $h_1^\perp$  and  $h_2^\perp$  go to zero, which permits simplifying expressions (28) and (29); also, the pair Hamiltonian can be analytically diagonalized for  $h_2^\perp = 0$ . So, by using the usual time-independent quantum mechanics perturbation theory up to second order in  $h_2^\perp$ , we can get the corresponding expanded eigenvalues. In this way we can write the following coupled equations:

$$\frac{2c[e^{\beta(D+\gamma_1^\perp)} - 1]}{(1-c)(D+\gamma_1^\perp)\mathcal{Z}_{1\perp}^f(0)} = \frac{\sum_i e^{-\beta\delta_i} \Gamma_i}{\mathcal{Z}_{2\perp}^p(0)}, \quad (30)$$

$$\frac{2e^{\beta(D+\gamma_1^\perp)}}{\mathcal{Z}_{1\perp}^f(0)} = \frac{e^{\beta(D+\gamma_2^\perp)}}{\mathcal{Z}_{2\perp}^p(0)} \left\{ 2 \cosh(\beta J\eta) + e^{\beta(J+D+\gamma_2^\perp)} \times [2 + e^{-2\beta J}] + e^{-\frac{\beta J}{2}} \left[ \cosh\left(\frac{\beta\Pi}{2}\right) - \frac{\kappa}{\Pi} \sinh\left(\frac{\beta\Pi}{2}\right) \right] \right\}, \quad (31)$$

where

$$\begin{aligned} & \sum_i e^{-\beta\delta_i} \Gamma_i \\ &= \frac{e^{-\beta[J-2(D+\gamma_2^\perp)]}}{J(1-\eta) - (D+\gamma_2^\perp)} + 2 \frac{e^{\beta[J+2(D+\gamma_2^\perp)]}}{-J(1-\eta) - (D+\gamma_2^\perp)} \\ &+ \frac{e^{-\beta[J\eta - (D+\gamma_2^\perp)]}}{-J(1-\eta) + (D+\gamma_2^\perp)} + 3 \frac{e^{-\beta\lambda_+ x_+^2}}{\lambda_+ + J\eta + D + \gamma_2^\perp} \end{aligned}$$

$$\begin{aligned}
 & + 3 \frac{e^{-\beta\lambda_-} x_-^2}{\lambda_- + J\eta + D + \gamma_2^\perp} + 2 \frac{e^{\beta(J\eta + D + \gamma_2^\perp)}}{J(1-\eta) + D + \gamma_2^\perp} \\
 & + 3x_+^2 \frac{e^{\beta(J\eta + D + \gamma_2^\perp)}}{-(J\eta + D + \gamma_2^\perp) - \lambda_+} \\
 & + 3x_-^2 \frac{e^{\beta(J\eta + D + \gamma_2^\perp)}}{-(J\eta + D + \gamma_2^\perp) - \lambda_-}, \quad (32)
 \end{aligned}$$

$$\mathcal{Z}_{1\perp}^f(0) = 1 + 2e^{\beta(D + \gamma_1^\perp)}, \quad (33)$$

$$\begin{aligned}
 \mathcal{Z}_{2\perp}^p(0) & = 4e^{\beta(D + \gamma_2^\perp)} \cosh(\beta J\eta) + e^{-\beta[J - 2(D + \gamma_2^\perp)]} \\
 & + 2e^{\beta[J + 2(D + \gamma_2^\perp)]} + 2e^{-\frac{\beta\kappa}{2}} \cosh\left(\frac{\beta\Pi}{2}\right), \quad (34)
 \end{aligned}$$

with

$$\begin{aligned}
 x_+ & = \sqrt{\frac{(\lambda_+ - b)}{\Pi}} \quad \text{and} \quad x_- = -\sqrt{\frac{(\lambda_- - a)}{\Pi}}, \quad (35) \\
 b & = \frac{2[J(2\eta + 1) - 2(D + \gamma_2^\perp)]}{3}, \\
 a & = \frac{J(-4\eta + 1) - 2(D + \gamma_2^\perp)}{3}, \quad (36) \\
 \Pi & = \sqrt{[J - 2(D + \gamma_2^\perp)]^2 + 8(J\eta)^2}, \\
 \kappa & = J - 2(D + \gamma_2^\perp), \quad \lambda_\pm = \frac{\kappa \pm \Pi}{2}.
 \end{aligned}$$

From Eqs. (30) and (31) one has the critical temperature for the perpendicular ordering  $m_\perp$ .

In addition, the first-order transition lines between the ordered phases (where  $m_\parallel \neq 0$  and  $m_\perp \neq 0$ ) are given when the corresponding free energies are equal, whereas they come from the ordered phases and the disordered phase when the free energies are the same as the free energy of the paramagnetic phase with  $m_\parallel = m_\perp = 0$ .

### B. Analytical results

Although in this approach, general results can only be achieved through a numerical analysis of the above equations, some additional analytical results are available in the limiting case  $D \rightarrow \infty$ . In that limit, we get for the reduced critical temperature  $t_c = \frac{k_B T_c}{J}$

$$t_c(D \rightarrow \infty) = \frac{2}{\ln\left(\frac{c}{c-2}\right)}. \quad (37)$$

Observe that the last expression does not depend on the anisotropy  $\eta$ , depending only on the coordination number  $c$  of the hypercube lattice. Therefore, in such limit, quantum effects are not relevant for the critical behavior. This fact is understandable because when we let  $D \rightarrow \infty$  in the Hamiltonian (1), the eigenvalues of the  $S^z$  operator can take only the values 1 and  $-1$ , since the high energetic cost prohibits that the eigenstates associated with zero eigenvalue could be accessed. Then, the Hamiltonian (1) reduces to the spin-1/2 Ising model, which is a classical one. Equation (37) gives  $t_c = 2.885$  in the two-dimensional limit, which should be compared to the exact result  $t_c = 2.269$  [45]. For the three-dimensional model, one has  $t_c = 4.932$ , comparable to Monte Carlo simulations  $t_c = 4.512$  [46].

TABLE I. Reduced critical temperatures  $t_c$  for the present model in some limiting cases, for the square ( $c = 4$ ) and simple cubic ( $c = 6$ ) lattices, according to exact results [21,45], Monte Carlo simulations [46], series expansion [47–49], the present values, and the usual (one-series) mean-field approach (mostly from Ref. [40]). The errors from Monte Carlo and series are in the next (not shown) two digits.

	$c = 4/c = 6$	Present	Usual MFA
$D \rightarrow \infty$	2.269/4.512 [46]	2.885/4.932	4/6
$D = 0, \eta = 0$	1.693 [47]/3.196 [48]	2.065/3.439	2.667/4
$D = 0, \eta = 1$	0 [21]/3.000 [49]	1.492/2.949	2.667/4

In the one-dimensional limit, the present approximation reproduces the exact result for the critical temperature,  $t_c = 0$ , even for the anisotropic Heisenberg model in the presence of the crystal field. In addition, for  $\eta = 0$  one further obtains the exact mean value of the quadrupole moment  $q$  in one dimension. This assures us that, at least for the 1D model, the present approach reproduces the exact results for all values of  $D$  and  $\eta$ . One should also say that for the spin-1/2 two-dimensional isotropic Heisenberg model (where the crystal field is unimportant since it is just a constant in the Hamiltonian) one also gets the exact result coming from the Mermin and Wagner theorem  $t_c = 0$  [21]. Despite the fact that for spin-1 one does not reproduce the Mermin and Wagner result for the two-dimensional model, we believe that the comparison depicted in Table I shows that the present pair approximation is clearly an improvement over the usual mean-field procedure previously done on this model.

### C. Location of tricritical and tetracritical points

As will be discussed in the next section, the model defined by the Hamiltonian (1) exhibits tricritical and tetracritical points in some particular ranges of the parameters of the Hamiltonian. In order to locate these multicritical points, besides the first- and second-order lines, we have resorted to a Landau-like expansion of the free energy (15). For the present case we arrive at the following expansion

$$\begin{aligned}
 \beta f & = f_0 + \frac{1}{2}a_2^\parallel(t, D, \eta)m_\parallel^2 + \frac{1}{4}a_4^\parallel(t, D, \eta)m_\parallel^4 + \frac{1}{6}a_6^\parallel m_\parallel^6 \\
 & + \frac{1}{2}a_2^\perp(t, D, \eta)m_\perp^2 + \frac{1}{4}a_4^\perp(t, D, \eta)m_\perp^4 + \frac{1}{6}a_6^\perp m_\perp^6, \quad (38)
 \end{aligned}$$

where  $f_0$  is a regular function and  $a_2^\parallel, a_4^\parallel, a_6^\parallel, a_2^\perp, a_4^\perp, a_6^\perp$  are coefficients depending on  $t, D, \eta$ . Tricritical points on the transition lines separating the parallel ordered and paramagnetic phases are given by

$$a_2^\parallel(t, D, \eta) = 0, \quad a_4^\parallel(t, D, \eta) = 0, \quad \text{and} \quad a_6^\parallel > 0.$$

The above coefficients have been analytically calculated and their expressions are given in the Appendix. On the other hand, tricritical points on the transition lines separating the perpendicular ordered and paramagnetic phases are given by

$$a_2^\perp(t, D, \eta) = 0, \quad a_4^\perp(t, D, \eta) = 0 \quad \text{and} \quad a_6^\perp > 0.$$

It turns out, as we shall see in the next section, that we do not find any tricritical point along this transition line.

Finally, the tetracritical point is given when

$$a_2^\parallel(t, D, \eta) = a_2^\perp(t, D, \eta) = 0 \quad \text{and} \quad a_4^\parallel > 0, \quad a_4^\perp > 0.$$

The expression for  $a_2^\perp$  is also given in the Appendix. In this particular case, the tetracritical point looks like a bicritical point in the temperature versus crystal-field plane, because we are considering zero external magnetic fields.

### III. NUMERICAL RESULTS

The numerical results of the one-dimensional and the three-dimensional versions of the model will be presented, including the thermodynamics and the global phase diagrams as a function of the parameters of the Hamiltonian. The results for the two-dimensional model are qualitatively similar to those for the cubic lattice.

#### A. One-dimensional model

For the 1D model,  $c = 2$ , the above equations give no ordering either along the  $z$  axis or in the  $xy$  plane for any values of  $\eta$  and  $D$ . One always has  $m_\parallel = m_\perp = 0$  with no transition at finite temperatures. This is indeed what one expects for this model. One should say that this is not accomplished by the simple mean-field approach, because it does not distinguish the dimension of the lattice, giving always a finite transition temperature for any value of  $c$ . Even more recent results obtained from the Green's function method were not able to describe such behavior, and the critical temperature of the 1D model only vanishes when  $\eta = 1$  and  $D = 0$  [50]. Note that when  $\eta = 0$ , one has the classical 1D Blume-Capel model which has no phase transition. As we increase  $\eta$  from zero, this increasing tends to destroy the  $z$ -axis order, which is already disordered, so no transition can be achieved in this case. In addition, for  $\eta = 0$  we get the exact free energy and the exact quadrupole moment  $q = \langle S_i^{z^2} \rangle$  as obtained from the transfer matrix formalism. The exact quadrupole as a function of temperature for  $\eta = 0$  is shown in Fig. 1(a) for several values of the crystal field. From what has been discussed above, we believe the present results for  $\eta > 0$ , shown in Figs. 1(b)–1(d), can be considered near to the exact ones. Unfortunately, in this case, the 1D model is nonintegrable for spin-1.

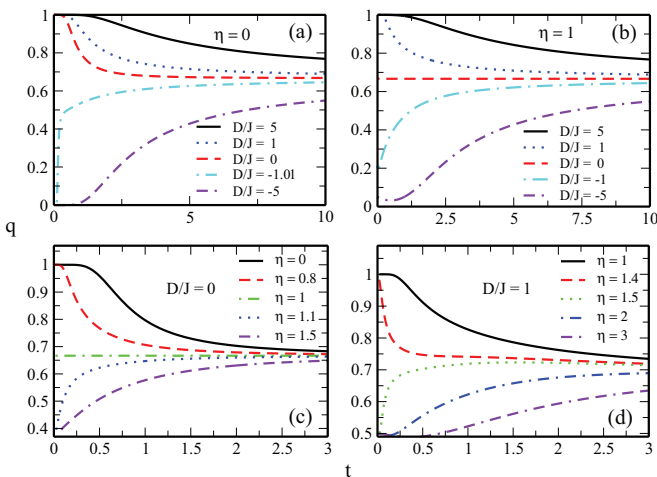


FIG. 1. (Color online) Quadrupole moment of the 1D model,  $c = 2$ , for several values of the Hamiltonian parameters.

It is interesting now to analyze the behavior of the 1D quadrupole and see what can be learned from the improved pair approximation. As Fig. 1(b) shows, for the isotropic model,  $\eta = 1$ , the quadrupole is ordered at zero temperature as soon as one has an easy-axis asymmetry for  $D/J > 0$ , while the quadrupole decreases when one has an easy plane for  $D/J < 0$ . For  $D/J = 0$ , the full isotropic case, the quadrupole is always disordered  $q = 2/3$ . The corresponding behavior of  $q$  for several values of the anisotropy  $\eta$  is shown in Fig. 1(c) for  $D/J = 0$ . Here the situation is quite similar to that of Fig. 1(b), with  $\eta < 1$  favoring the  $z$  axis and  $\eta > 1$  favoring the  $xy$  plane. In Fig. 1(d) for  $D/J = 1$ , which already favors the  $z$  axis, one can see a higher value of  $\eta$  (in this case  $1.4 < \eta < 1.5$ ) in order to favor the  $xy$  plane.

#### B. Three-dimensional model

In this section, we present the numerical results of the behavior of the magnetization  $m = \langle S_j^z \rangle$ , the pair correlation function on the  $xy$  plane  $\langle S_i^x S_j^x + S_i^y S_j^y \rangle$ , and the global phase diagrams as functions of the parameters of the Hamiltonian for the 3D model. The results for the two-dimensional model are qualitatively the same.

##### 1. Magnetization and pair correlation function

In Fig. 2 we show the parallel and perpendicular magnetizations as a function of the reduced temperature  $t = k_B T/J$ , for several values of  $\eta$ , for the 3D model and  $D/J = 0$ . In Fig. 2(a), we have  $\eta < 1$  and the stable phase is the one with an Ising-like ordering along the  $z$  direction and exhibiting a continuous phase transition as the temperature is increased. One also notes that as the anisotropy is decreased, the quantum fluctuations increase and the critical temperature is lowered. The spin components tend to lie more in the  $xy$  plane as  $\eta \rightarrow 1$ . On the other hand, in Fig. 2(b), where  $\eta > 1$ , the stable phase is the one with a perpendicular ordering. Now, by increasing  $\eta$ , the easy-plane tendency of the ordering is enhanced and, as a consequence, the critical temperature is also increased. However, one can see a reentrant behavior where a second continuous transition takes place at low temperatures. This reentrancy will become clearer when discussing the

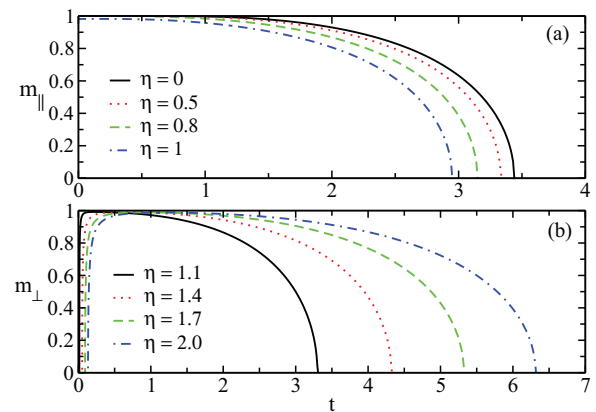


FIG. 2. (Color online) (a) Parallel  $m_\parallel$  and (b) perpendicular  $m_\perp$  magnetizations as a function of the reduced temperature  $t = k_B T/J$ , for  $D/J = 0$ ,  $c = 6$ , and several values of the anisotropy  $\eta$ .

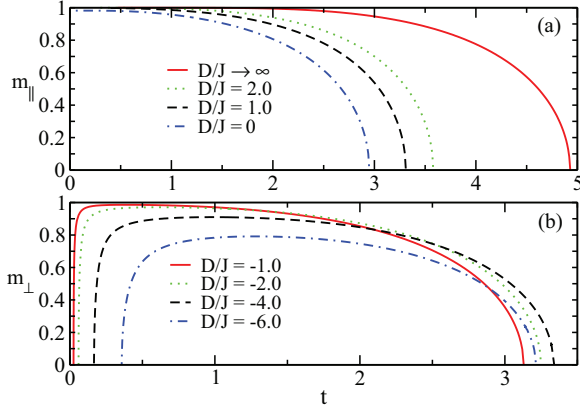


FIG. 3. (Color online) (a) Parallel  $m_{\parallel}$  and (b) perpendicular  $m_{\perp}$  magnetizations as a function of the reduced temperature  $t = k_B T/J$ , for  $\eta = 1$ ,  $c = 6$ , and several values of the crystal field  $D/J$ .

phase diagrams. Figure 3 depicts the magnetizations for  $\eta = 1$  and various values of the crystal field. In this case, two continuous transitions are seen for negative values of  $D$ . These reentrancies are not found in the usual mean-field approach.

The nearest-neighbor pair correlation function in the  $xy$  plane is shown in Fig. 4 for  $D/J = 0$  and various values of  $\eta$ . For  $\eta > 1$ , the easy-plane situation, this correlation function decreases as the temperature increases, because the system is already ordered in the plane. On the other hand, for  $\eta < 1$ , the easy-axis case, the in-plane correlation function increases as the temperature increases, since the temperature tends to destroy the order along the  $z$  direction, favoring in this case the  $xy$  plane. The inset in Fig. 4(a) shows the special case  $\eta = 1$ , where we have a coexistence of both ordered phases, along the  $z$  direction and in the  $xy$  plane. The pair correlation functions behave differently in each phase, becoming equal at the tetracritical temperature (see discussion below).

2. Global phase diagrams

Figure 5 displays the global phase diagram in the reduced critical temperature versus reduced crystal-field plane, in the

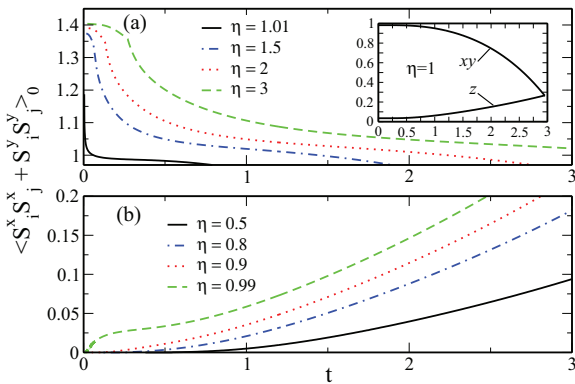


FIG. 4. (Color online) In-plane nearest-neighbor pair correlation function as a function of the reduced temperature for the 3D model and  $D/J = 0$  for several values of  $\eta$ . (a)  $\eta > 1$  and (b)  $\eta < 1$ . The inset in (a) shows the results for  $\eta = 1$  for the ordered phase in the  $z$  direction and  $xy$  plane.

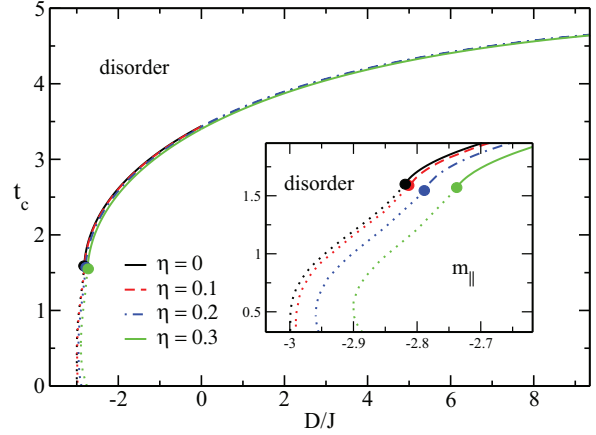


FIG. 5. (Color online) Global phase diagram in the reduced temperature versus crystal field for several values of the anisotropy  $\eta \leq 0.3$ , in the 3D lattice with  $c = 6$ . The dotted lines refer to first-order transitions and the others lines (continuous, dashed, and dotted-dashed) refer to second-order phase transitions. The circles represent the tricritical points. The transition is always from the stable parallel ordered phase with  $m_{\parallel} \neq 0$  to the disordered phase. The inset shows the low-temperature region on a finer scale.

3D limit, for several values of the anisotropy  $\eta$ . One can see that as soon as  $\eta < 0.33$  the phase diagram is quite similar to that of the classical Blume-Capel model, presenting second- and first-order transition lines separated by a tricritical point. In the limit  $D/J \rightarrow \infty$  all curves go to the same result  $t_c = 4.932$ , as discussed in the text. Apart from the reentrancy at low temperatures, which is clearly depicted in the inset, for this range of anisotropy the quantum effects seem not to be enough to change the character of the transition, and the perpendicular ordered phase is never stable. The anisotropy can only stabilize the perpendicular phase when  $\eta > 0.33$ . This is in contrast to the simple mean-field approach, where the perpendicular order is always stable as soon as  $\eta > 0$  [40].

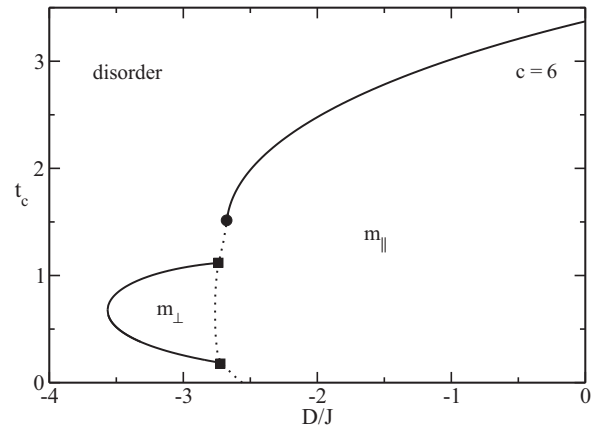


FIG. 6. Global phase diagram in the reduced temperature versus crystal-field plane for  $\eta = 0.4$ , in the 3D lattice with  $c = 6$ . The continuous lines refer to second-order phase transitions and the dotted line refers to first-order transition. The circle represents the tricritical point and the squares represent the critical endpoints.  $m_{\parallel}$  is the parallel ordered phase and  $m_{\perp}$  is the perpendicular ordered phase.

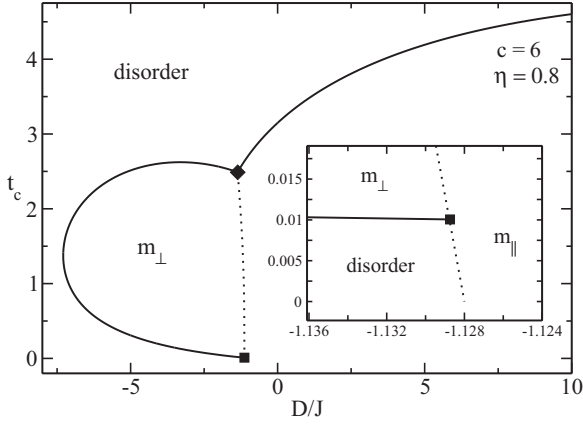


FIG. 7. Global phase diagram in the reduced temperature versus crystal-field plane for  $\eta = 0.8$ , in the 3D lattice with  $c = 6$ . The continuous lines refer to second-order phase transitions and the dotted line refers to first-order transition. The squares represent the low-temperature critical endpoint and the diamond represents the tetracritical point.  $m_{\parallel}$  is the parallel ordered phase and  $m_{\perp}$  is the perpendicular ordered phase. The inset shows a closer view of the low-temperature region.

For  $0.33 < \eta < 0.49$  the phase diagram looks like the one shown in Fig. 6. In addition to the tricritical point, one has two critical endpoints in the first-order transition line separating the parallel and perpendicular ordered phases. As  $\eta$  increases, the tricritical and the high-temperature critical endpoint approach one another and eventually, for  $\eta > 0.49$ , they coalesce in a tetracritical point. The phase diagram in this range of anisotropy is depicted in Fig. 7.

For  $\eta = 1$  the first-order transition line separating the perpendicular and the parallel phases is a straight vertical line at  $D/J = 0$ , as shown in Fig. 8 together with a comparison with the usual mean-field approximation (or one-spin approach) [40]. One can see that the critical temperature from the pair approximation is systematically below the mean-field results

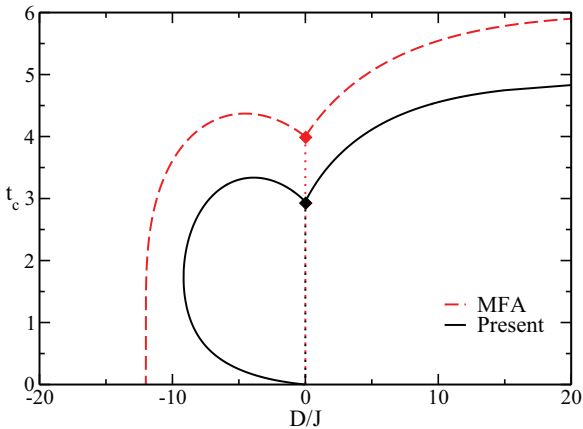


FIG. 8. (Color online) Phase diagram in the reduced temperature versus crystal-field plane for  $\eta = 1$ , in the 3D lattice with  $c = 6$ , according to the present approach in comparison to the MFA. The continuous and dashed lines refer to second-order phase transitions and the dotted lines refer to first-order transition. The diamonds represent the the tetracritical point.

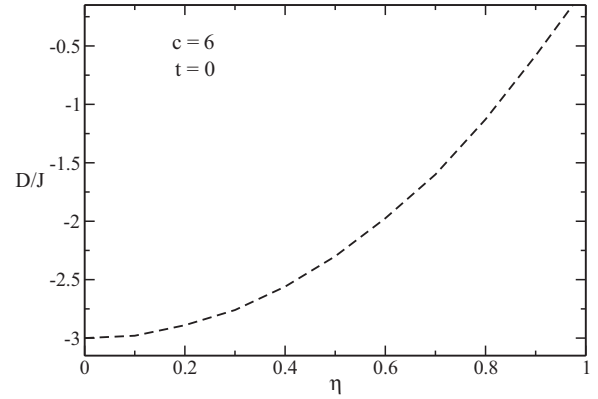


FIG. 9. Reduced crystal field  $D/J$  as a function of the anisotropy  $\eta$ , at zero temperature  $T = 0$ , for the 3D model.

by taking just one-spin cluster. The reentrancy only occurs for the pair approximation. Similar results are obtained for other values of  $\eta > 1$ , with the slope of the first-order transition line between the ordered phases becoming positive in this range.

All of the above results refer to the 3D model with coordination number  $c = 6$ . The same holds for the two-dimensional model. It means that in this case, for spin  $S = 1$ , one does not get the Mermin and Wagner result  $T_c = 0$  for  $\eta = 1$  and  $D = 0$ . However, we believe the approach is suitable for the 3D system, mainly when we compare the critical temperatures, as depicted in Table I.

### C. Quantum phase diagram $T = 0$

From Figs. 5–8, we note that for each anisotropy there exists a value for the crystal field  $D/J$  in which there is a transition at  $t = 0$ . This transition happens to be of first order and it is illustrated in Fig. 9. One can find neither a second-order quantum phase transition nor a quantum tricritical point according to the present pair procedure, in contrast to the simple mean-field approach where there is always a quantum phase transition at zero temperature. It should be stressed, however, that there is a rigorous proof of the existence of only first-order phase transitions at low temperature and large anisotropy for the  $XXZ$  model [51].

### IV. CONCLUDING REMARKS

The anisotropic spin-1  $XXZ$  quantum Heisenberg model in a crystal field has been studied according to a variational approach for the free energy by using a pair approximation. This procedure enables one to get the ordering along the  $z$  direction and in the  $xy$  plane as well. Earlier pair-like approaches on the same system could only take into account the parallel ordering.

As expected, the one-dimensional model has no phase transition and the quadrupole moment so obtained is expected to be close to the exact one for  $\eta > 0$ . So, contrary to the simple mean-field approximation, the present pair approach can distinguish the dimensionality of the lattice and much more novel information is obtained regarding the free energy and quadrupole moment for  $c = 2$ .

From the free energies one gets the complete phase diagrams for dimensions greater than unity, which are indeed

much richer than those from the simple mean-field procedure. The diagrams exhibit second- and first-order transition lines and tricritical and tetracritical points, as well as critical endpoints. Although for the spin-1 case we do not reproduce the Mermin-Wagner theorem in the two-dimensional case, we believe the results are appropriate for the three-dimensional model. Of course, as it is still a mean-field approach, it should be necessary to use more reliable methods to corroborate the reentrancies observed in some range of the Hamiltonian parameters.

#### ACKNOWLEDGMENTS

The authors thank CNPq, FAPEMIG, and CAPES (Brazilian agencies) for financial support. Fruitful discussions with S. L. de Queiroz and R. Stinchcombe are also gratefully acknowledged.

#### APPENDIX

In this Appendix we present the expressions for the coefficients  $a_2^{\parallel}(t, D, \eta)$ ,  $a_4^{\parallel}(t, D, \eta)$ , and  $a_2^{\perp}(t, D, \eta)$  appearing in the Landau expansion for the free energy [Eq. (38)] in

Sec. II C. Before writing these coefficients, we will define the following variables:

$$\begin{aligned} \epsilon &= \frac{\mathcal{Z}_{2\parallel}^p(0)}{2e^{\beta(D+\gamma_2^{\parallel})}[\cosh(\beta J\eta) + 2e^{\beta(J+D+\gamma_2^{\parallel})}]}, \\ A &= \frac{2e^{\beta(D+\gamma_1^{\parallel})}}{\mathcal{Z}_{1\parallel}^f(0)}, \quad B = \frac{A}{6} - \frac{A^2}{2}, \\ I &= e^{\beta(D+\gamma_2^{\parallel})}[\cosh(\beta J\eta) + 8e^{\beta(J+D+\gamma_2^{\parallel})}], \end{aligned}$$

where  $\mathcal{Z}_{1\parallel}^f(0)$  and  $\mathcal{Z}_{2\parallel}^p(0)$  are given by Eqs. (26) and (27). So, we can write

$$\begin{aligned} a_2^{\parallel} &= \frac{(1-c)}{2A} - \frac{c\epsilon}{2}, \\ a_4^{\parallel} &= \frac{B(c-1)}{4A^4} - \frac{cI\epsilon^4}{2\mathcal{Z}_{2\parallel}^p(0)} + \frac{c\epsilon^2}{4}, \\ a_2^{\perp} &= \frac{2c[e^{\beta(D+\gamma_1^{\perp})} - 1]}{(1-c)(D+\gamma_1^{\perp})\mathcal{Z}_{1\perp}^f(0)} - \frac{\sum_i e^{-\beta\delta_i} \Gamma_i}{\mathcal{Z}_{2\perp}^p(0)}, \end{aligned}$$

where  $\mathcal{Z}_{1\perp}^f(0)$ ,  $\mathcal{Z}_{2\perp}^p(0)$ , and  $\sum_i e^{-\beta\delta_i} \Gamma_i$  are given by Eqs. (33), (34), and (32), respectively.

- 
- [1] G. Giovannetti *et al.*, *Nat. Commun.* **2**, 398 (2011).
  - [2] T. R. Kirkpatrick and D. Belitz, *Phys. Rev. B* **85**, 134451 (2012).
  - [3] M. Uhlarz, C. Pfleiderer, and S. M. Hayden, *Phys. Rev. Lett.* **93**, 256404 (2004).
  - [4] J. Hertz, *Phys. Rev. B* **14**, 1165 (1976).
  - [5] S. L. Sondhi *et al.*, *Rev. Mod. Phys.* **69**, 315 (1997).
  - [6] K. R. Hazzard, *Quantum Phase Transitions in Cold Atoms and Low Temperature Solids* (Springer, New York, 2011).
  - [7] L. D. Carr, *Understanding Quantum Phase Transitions*, Series in Condensed Matter Physics (CRC, Boca Raton, FL, 2010).
  - [8] D. Bitko, T. F. Rosenbaum, and G. Aeppli, *Phys. Rev. Lett.* **77**, 940 (1996).
  - [9] B. Keimer *et al.*, *Phys. Rev. B* **46**, 14034 (1992).
  - [10] T. Mikasawa, Y. Yamaji, and M. Imada, *J. Phys. Soc. Jpn.* **78**, 084707 (2009).
  - [11] S. Sachdev, *Quantum Phase Transitions* (Cambridge University, Cambridge, England, 1999).
  - [12] W. Shiramura *et al.*, *J. Phys. Soc. Jpn.* **67**, 1548 (1998).
  - [13] P. Pfeuty, *Ann. Phys. (NY)* **57**, 79 (1970).
  - [14] J. B. Kogut, *Rev. Mod. Phys.* **51**, 659 (1979).
  - [15] D. C. Carvalho, L. M. Castro, and J. A. Plascak, *Physica A* **391**, 1149 (2012).
  - [16] A. S. T. Pires, *Sol. State Comm.* **100**, 791 (1996).
  - [17] A. S. T. Pires, *J. Magn. Magn. Mater.* **323**, 1977 (2011).
  - [18] V. S. Abgaryan *et al.*, *Phys. Scr.* **83**, 055702 (2011).
  - [19] M. E. Fisher, *Am. J. Phys.* **32**, 343 (1964).
  - [20] H. Bethe, *Z. Physik A* **71**, 205 (1931).
  - [21] N. D. Mermin and H. Wagner, *Phys. Rev. Lett.* **17**, 1133 (1966).
  - [22] J. H. Van Vleck, *Phys. Rev.* **41**, 208 (1932).
  - [23] J. H. Van Vleck, *The Theory of Electric and Magnetic Susceptibilities* (Oxford University, Oxford, 1932).
  - [24] H. Bethe, *Ann. Physik* **3**, 133 (1929).
  - [25] *Crystalline Electric Field and Structural Effect in f-Electron Systems*, edited by J. E. Crow, R. P. Gruertin, and T. W. Mihalisin (Plenum, New York, 1980).
  - [26] C. Pfleiderer and A. D. Huxley, *Phys. Rev. Lett.* **89**, 147005 (2002).
  - [27] M. Blume, *Phys. Rev.* **141**, 517 (1966).
  - [28] H. W. Capel, *Physica* **32**, 966 (1966).
  - [29] J. A. Plascak, J. G. Moreira, and F. C. S. Barreto, *Phys. Lett. A* **173**, 360 (1993).
  - [30] D. Peña Lara and J. A. Plascak, *Mod. Phys. Lett. B* **10**, 1067 (1996).
  - [31] D. Peña Lara and J. A. Plascak, *Int. J. Mod. Phys.* **12**, 2045 (1998).
  - [32] A. K. Jain and D. P. Landau, *Phys. Rev. B* **22**, 445 (1980).
  - [33] J. A. Plascak and D. P. Landau, *Phys. Rev. E* **67**, 015103(R) (2003).
  - [34] C. J. Silva, A. A. Caparica, and J. A. Plascak, *Phys. Rev. E* **73**, 036702 (2006).
  - [35] J. C. Xavier, F. C. Alcaraz, D. Peña Lara, and J. A. Plascak, *Phys. Rev. B* **57**, 11575 (1998).
  - [36] V. A. Schmidt and S. A. Friedberg, *Phys. Rev.* **1**, 2250 (1970).
  - [37] J. Oitmaa and C. J. Hamer, *Phys. Rev. B* **77**, 224435 (2008).
  - [38] M. Blume, V. J. Emery, and R. B. Griffiths, *Phys. Rev. A* **4**, 1071 (1971).
  - [39] G. P. Taggart, R. A. Tahir-Kheli, and E. Shiles, *Physica* **75**, 234 (1974).
  - [40] M. R. H. Khajepour, Yung-Li Wang, and Robert A. Kromhout, *Phys. Rev.* **12**, 1849 (1975).
  - [41] Kok-Kwei Pan and Yung-Li Wang, *Phys. Rev. B* **51**, 3610 (1995).
  - [42] J. Strečka, J. Dely, and L. Čanová, *Chinese J. Phys.* **46**, 329 (2008).

- [43] H. Falk, *Am. J. Phys.* **38**, 858 (1970).
- [44] L. G. Ferreira, S. R. Salinas, and M. J. Oliveira, *Phys. Status Solidi B* **83**, 229 (1977).
- [45] L. Onsager, *Phys. Rev.* **65**, 117 (1944).
- [46] A. M. Ferrenberg and D. P. Landau, *Phys. Rev. B* **44**, 5081 (1991).
- [47] I. G. Enting, A. J. Guttmann, and I. Jensen, *J. Phys. A: Math. Gen.* **27**, 6987 (1994).
- [48] P. Butera and M. Comi, *Phys. Rev. B* **65**, 144431 (2002).
- [49] H. E. Stanley and T. A. Kaplan, *Phys. Rev. Lett.* **17**, 913 (1966).
- [50] C. C. Song, Y. Cheng, and M.-W. Liu, *Physica B* **405**, 439 (2010).
- [51] R. W. Robinson, *Commun. Math. Phys.* **14**, 195 (1969).